Description of bulk properties of charged pions, kaons, and (anti)protons in Au+Au collisions from the STAR experiment in the Beam Energy Scan program within the improved HIJING code: Role of initial-state interactions

Khaled Abdel-Waged ●* and Nuha Felemban ●

Physics Department, Faculty of Applied Science, Umm Al-Qura university, P.O. Box 10471, Makkah 21955, Saudi Arabia

We have investigated the production yields of charged pions, kaons, and (anti)protons (restricted to midrapidity of $|y| < 0.1$) in Au+Au collisions at $\sqrt{s_{NN}} = 7.7$, 11.5, 19.6, 27, and 39 GeV, from the STAR experiment in the Beam Energy Scan (BES) program at the Relativistic Heavy Ion Collider (RHIC), within an improved heavy-ion jet interaction generator (ImHIJING) code plus a relativistic transport (ART) model. Improvements of the dynamical content of ImHIJING code include (i) sampling of initial momenta of nuclear ground state, (ii) a Regge cascade for initial-state interaction effects, and (iii) an advanced popcorn mechanism for baryon production. It is found that the implementation of initial-state interactions in the ImHIJING+ART model is crucial for the description of collision centrality dependence of bulk hadron observables in peripheral and semicentral ($\approx10\%$–70%) Au+Au collisions at $\sqrt{s_{NN}} > 11.5$ GeV.

I. INTRODUCTION

Recent measurements by STAR Collaboration [1] within the Relativistic Heavy Ion Collider (RHIC) program provide high precision data of identified particles $\pi^{\pm}$, $K^{\pm}$, and (anti)protons at mid-rapidity ($|y| < 0.1$) in Au+Au collisions in the Beam Energy Scan (BES) at $\sqrt{s_{NN}} = 7.7$, 11.5, 19.6, 27, and 39 GeV. The bulk properties of produced particles such as transverse momentum (p_T) spectra, multiplicity density (dN/dy), and particle ratios may provide insight into the particle production mechanisms from the lowest possible energy to the highest possible BES, thereby looking for the signature of the quantum chromodynamic (QCD) phase boundary.

The production mechanisms of particles from the first nucleon-nucleon (NN) interactions stage to the final state interactions may shed light on the theoretical understanding of the dynamical evolution of relativistic heavy-ion collisions. To explore these evolutionary processes, many microscopic hadronic transport models are used to simulate heavy-ion collisions, such as relativistic quantum molecular dynamics (RQMD) [2], ultrarelativistic quantum molecular dynamics (UrQMD) [3], a relativistic cascade (ARC) [4], a relativistic transport (ART) [5] and a multiphase transport (AMPT) [6] models.

The AMPT model [6] has been developed, based on the resonance, strings, and minijets degrees of freedom, to give a coherent description of the dynamics of relativistic heavy-ion collisions. It consists of four main components: (i) the initial conditions for the strings and minijet partons, obtained from

the HIJING model [7]; (ii) a mechanism for partonic energy loss during the first few fm/c of the nuclear collisions, using Zhang's parton cascade (ZPC) [8] model of parton scatterings; (iii) a hadronization process based on the Lund string framentation scheme [9–11], using PYTHIA 5.4 [12]; and (iV) hadron rescatterings described by the ART model [5].

Recently, the AMPT model has been used to study the STAR data of p_T spectra, dN/dy, and particle ratios of charged pions, kaons, and (anti)protons, produced in Au+Au collisions at $\sqrt{s_{NN}} = 7.7$, 27, and 200 GeV [13]. For this study, three different sets of parameters were applied for both the default and string melting versions of the AMPT model [14]. It was shown in Ref. [13] that neither version of the AMPT model was able to describe the bulk properties of the measured data using a single set of parameters.

In the present work, we attempt a further investigation of the recent STAR data [1], of $\pi^{\pm}$, $K^{\pm}$, and $p^{\pm}$ in Au+Au collisions at $\sqrt{s_{NN}} = 7.7$, 11.5, 19.6, 27, and 39 GeV, in the framework of the improved HIJING code [15]. As will be explained below, for a comprehensive description of STAR data of bulk hadron production, several ingredients are introduced in the standard HIJING code. The new features are (i) sampling of Fermi motion of the nuclear ground state, (ii) a Regge cascade for initial-state interactions [16], and (iii) an advanced popcorn for baryon production mechanisms [17]. This improved version will be denoted as HIJING/AP/Rcas. A meaningful comparison of STAR data [1] requires the introduction of final state interactions. Similar to AMPT code [6], we adopt the ART model [5] of hadron rescattering.

The paper is organized as follows: Section II defines the basic ingredients of the HIJING/AP/Rcas+ART model. In Sec. III we confront the model with measurements from

*khelwagd@yahoo.com

STAR [1] experiments. Finally, in Sec. IV we present our conclusions.

II. DESCRIPTION OF THE HIJING/AP/Rcas+ART model

Here we outline the basic ideas of the HIJING/AP/Rcas+ART model. The details of HIJING/AP/Rcas and ART are described in Refs. [5,15,16,18,19]. Here we concentrate on those points which are important for understanding the results discussed in Sec. III.

  (i) Initially, the positions of the nucleons of the two colliding nuclei are sampled according to the three-parameter Saxon-Woods distribution.

 (ii) To initialize the nuclei in momentum space, the Regge cascade algorithm [18,19] is used [see steps (v) and (vi) below], by replacing the number of interacting nucleons ($N'_{A(B)}$) with the mass number A (B) of the projectile (target). The algorithm ensures that the momenta of nucleons give the Thomas-Fermi distribution, and energy-momentum conservation is applied.

(iii) The collision proceeds via N-primary interactions between N_A and N_B nucleons. The number of participant nucleons ($N_{\text{part}} = N_A + N_B$) is sampled according to the eikonal formalism of the HIJING code [7].

 (iv) As described by Regge cascade [18,19], initial-state interactions arise due to simultaneous interactions of a primary interacting nucleon with other noninteracting ones from the projectile/target. In nucleus-nucleus ($A + B$) collisions, the probability of involving the ith noninteracting (secondary) nucleon by the jth primary one, at the impact parameter distance $b_{ij} = \sqrt{(b_x + x_i - x_j)^2 + (b_y + y_i - y_j)^2}$, is given by

$$\phi = C \exp\left(-b_{ij}^2/r_0^2\right), \qquad (1)$$

where $r_0 = 1.4$ fm is the mean interaction radius. The parameter C determines the strength of initial-state interactions. Note that, in the case of $C = 0$, ϕ reduces to the eikonal case, with no Regge cascading.

 (v) In the Regge approach [18,19], the light cone variables $W_A^+ = (E_i + p_{zi})$ and $W_B^- = (E_j - q_{zj})$ are used for a projectile nucleus (A) moving out along the $+z$ axis and the target nucleus (B) along the $-z$ one, where E_i (E_j) and p_{zi} (q_{zj}) are the initial energy and longitudinal momentum of the ith (jth) wounded nucleon. The corresponding total energy and momentum are given by $E^0 = \sum_{i=1}^{N'_A} E_i$ and $p_z^0 = \sum_{i=1}^{N'_B} p_{zi}$, respectively, where $N'_{A(B)}$ is the number of wounded nucleons (which are determined either from the eikonal formalism or Regge cascade) from the projectile/target. The final momentum can then be determined in terms of the probability distribution

$$P(x_i'^+, p_{Ti}') \propto \prod_{i=1}^{N'_{A(B)}} \exp\left[-\frac{p_{Ti}'^2}{\langle p_T^2 \rangle}\right] \exp\left[-\frac{\left(x_i'^+ - \frac{1}{N'_{A(B)}}\right)^2}{d^2}\right] \delta\left(\sum_{i=1}^{N'_{A(B)}} p_{Ti}'\right) dp_{Ti}' \delta\left(1 - \sum_{i=1}^{N'_{A(B)}} x_i'^+\right) dx_i'^+, \qquad (2)$$

The fractional momentum ($x_i'^+$) of the wounded nucleon is chosen with a mean $\mu = 1/N'_{A(B)}$ and a width $d = \epsilon/N'_{A(B)}$. In Eq. (2), the average transverse momentum ($\langle p_T^2 \rangle$) and ϵ are free parameters of the model.

(vi) By applying energy-momentum conservation, the final momenta of the ith and jth wounded nucleons are given in terms of ($x_i'^+, p_{Ti}'$), as

$$p_{zi}' = \left(W_A'^+ x_i'^+ - \frac{m_{Ti}'^2}{x_i'^+ W_A'^+}\right)\Big/2, \qquad (3)$$

$$q_{zj}' = -\left(W_B'^- x_j'^- - \frac{\mu_{Tj}'^2}{x_j'^- W_B'^-}\right)\Big/2, \qquad (4)$$

where $m_{Ti}'^2 = m_i^2 + p_{Ti}'^2$, $\mu_{Tj}'^2 = \mu_j^2 + q_{Tj}'^2$, and m_i (μ_j) is the mass of the ith (jth) secondary interacting nucleon from $A(B)$. In Eqs. (3) and (4),

the light cone variables $\acute{W}_A^+$ and $\acute{W}_B^-$ are given by

$$\acute{W}_A^+ = \frac{(W_0^- W_0^+ + \alpha - \beta + \sqrt{\Delta})}{2W_0^-}, \qquad (5)$$

$$\acute{W}_B^- = \frac{(W_0^- W_0^+ - \alpha + \beta + \sqrt{\Delta})}{2W_0^+}, \qquad (6)$$

where

$$W_0^+ = \left(E_A^0 + E_B^0\right) + \left(p_{zA}^0 + q_{zB}^0\right),$$
$$W_0^- = \left(E_A^0 + E_B^0\right) - \left(q_{zA}^0 + q_{zB}^0\right),$$
$$\alpha = \sum_{i=1}^{N_A} \frac{\acute{m}_{Ti}^2}{\acute{x}_i^+}, \qquad \beta = \sum_{j=1}^{N_B} \frac{\acute{\mu}_{Tj}^2}{\acute{y}_j^-},$$

and

$$\Delta = (W_0^- W_0^+)^2 + \alpha^2 + \beta^2 - 2W_0^- W_0^+ \alpha$$
$$- 2W_0^- W_0^+ \beta - 2\alpha\beta.$$

(vii) The Regge cascade [16,20] induces both collective cascade and nuclear modifications of nucleons that participated in the primary interactions inside the projectile/target nucleus. In particular, nucleons taking part in the primary interactions suffer energy loss due to cascading with other noninteracting ones. Thus, the energy/momentum of the minijet partons and excited strings, produced from hard and soft NN scatterings, respectively, is expected to be reduced from their initial distributions in the default HIJING code. This implies that, in contrast to standard HIJING [7], HIJING/Rcas [16,20] incorporates in-medium effects in the initial stage of the interactions.

(viii) Multiparticle production from soft ($\sqrt{s_{NN}} \leqslant 10$ GeV) and hard ($\sqrt{s_{NN}} > 10$ GeV) NN collisions in HIJING/AP/Rcas code is modeled as follows. For each hard interaction, characterized by inclusive jet cross section (σ_{jet}), the kinetic variables of gluon-gluon scatterings are determined by the PYTHIA 6.4 model [21]. Produced gluons are ordered in their rapidities and then connected with their valence quarks or diquarks to form string systems. The scheme for accompanying soft interactions is determined by the advanced popcorn scenario [17] of baryon production. It is assumed that a vertex pair q'_2-$\bar{q}'_2$ is produced inside a color fluctuation region spanned by a "curtain" pair q_1-$\bar{q}_1$. The string can break if a $q_1\bar{q}'_2$-$q_1\bar{q}'_2$ is produced and pulled apart by the string tension. In contrast to the default diqurrk/simple-popcorn mechanism [22,23] adopted by HIJING [7,14] type models, the advanced popcorn model allows for several breakups in the color fluctuation region, creating one or several mesons in between the $B\bar{B}$. The probability to find such a curtain pair q_1-$\bar{q}_1$ with transverse mass $M_\perp$ of diquark and meson is estimated by [17]

$$|\Gamma|^2 \sim \exp(-2M_{\perp q_1}/k_0). \qquad (7)$$

In the implementation, the average transverse momentum $\langle M_{\perp q_1} \rangle$ for light and strange quarks is determined by two parameters [17]

$$\beta_u = 2\langle M_{\perp u}\rangle/k_0 \quad \text{and} \quad \Delta\beta = \beta_s - \beta_u. \qquad (8)$$

In the string decay, the production rate of heavy Q'-$\bar{Q}'$ pairs related to light q'-$\bar{q}'$ pairs is determined via the Schwinger formulas [24]:

$$\gamma_{Q'\bar{Q}'} = \frac{P_{Q'-\bar{Q}'}}{P_{q'-\bar{q}'}} = \exp\big[-\pi\big(\mu_{\perp Q'}^2 - \mu_{\perp q'}^2\big)/k_0\big]. \qquad (9)$$

where $2\mu_{\perp q'} = 2\sqrt{m_{q'}^2 + p_\perp^2}$ is the transverse mass of the pair of quarks with mass $m_{q'}$ and transverse momentum $p_\perp$. For the vacuum string tension value $k_0 = 1$ GeV fm^{-1}, the above equation results in a suppression of strange quarks by a factor of 0.3 with respect to light quarks, which is the default setting in the PYTHIA 6.4 routines [21]. The model contains six parameters that govern baryon multiplicities: (i) the ratio of production rates of diquark-antidiquark

to quark-antiquark pairs (diquark-quark suppression factor), $\gamma_{q'q'} = P_{q'q'-\bar{q}'\bar{q}'}/P_{q'-\bar{q}'} = \mathrm{PARJ}(1)$; (ii) the ratio of production rates of strange to nonstrange quark pairs (strangeness suppression factor), $\gamma_s = P_{s-\bar{s}}/P_{q'-\bar{q}'} = \mathrm{PARJ}(2)$; (iii) the average transverse momentum of light quarks, $\beta_u = \mathrm{PARJ}(8)$; (iv) the average transverse momentum of strange quarks, $\Delta\beta = \mathrm{PARJ}(9)$; (v) suppression of diquark vertices with large fractional momentum, $\Delta a = \mathrm{PARJ}(10)$; and (vi) suppression of the first rank (counting from the string ends) light baryon, $e^{-\rho}$ PARF(192).

(ix) The produced quarks and antiquarks recombine with neighboring partons into (pre)hadronic state after a formation time $\tau_f = 0.7$ fm/c (in the rest frame of the string). Hadrons acquire longitudinal momentum (p_z) determined by the Lund symmetric fragmentation function [25]:

$$f(z) \propto \frac{1}{z}(1-z)^\alpha \exp\left(-\frac{bm_\perp^2}{z}\right), \qquad (10)$$

here z is the light-cone longitudinal momentum fraction of the produced hadron with transverse momentum $m_\perp$. The transverse momentum of a hadron is given by a vertex diquark p_T kick characterized by a Gaussian width $\sigma_{q'q'}$, with $\sigma_{q'q'} = \mathrm{PARJ}(21)$ [21].

(x) The final state interactions are described by the relativistic transport ART model [5]. The model covers baryon and meson resonances as well as interactions among them for collision dynamics up to Alternating Gradient Synchrotron (AGS) energies ($E_{\mathrm{lab}} = 1$–15 GeV/A). These include (i) π, ρ, ω, η, K, K^*, and ϕ for mesons, (ii) N, Δ, $N^*(1440)$, $N^*(1535)$, Λ, Σ, Ξ, and Ω for baryons and antibaryons, (iii) $N\bar{N}$ and $(N\Delta N^*)(\bar{N}\bar{\Delta}\bar{N}^*)$ annihilation, an (iv) mean-field potentials for nucleons and kaons. In the present study, we turned off the potentials in the ART model [5] because their effects are found to be small in heavy-ion collisions at BES energies.

In Fig. 1 we display a schematic representation of the HIJING/AP/Rcas+ART described above. As already described above, the Regge cascade recipe is introduced to induce both collective cascade and nucleon energy loss before minijet production and string fragmentation as a convenient step in lowering the high partonic energy density during the first few fm/c of Au+Au collisions. As one can see in Fig. 2, HIJING/AP with Regge cascade (thick solid lines) increases the yield of protons and lowers the number of newly produced $\pi^\pm$ and $K^\pm$ particles, compared to HIJING/AP, for $\langle N_{part} \gg 20$ (which corresponds to $\approx 0\%$–70% centrality). This indicates that the abundances of the newly produced particles are sensitive to the energy loss of the initial colliding nucleons, i.e., to the fraction of their kinetic energy which will be converted into minijets/strings and subsequently produce hadrons.

To interpret the results presented in Fig. 2, we have analyzed the time evolution of local baryon and energy densities at different impact parameters. In the lower panel of Fig. 3 we
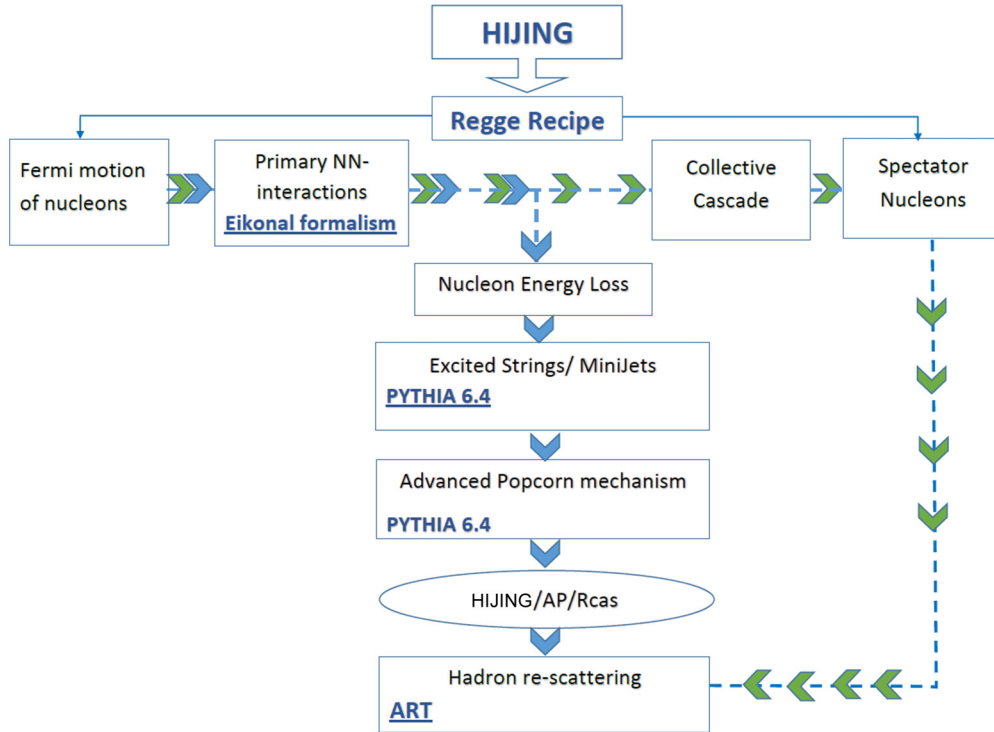
FIG. 1. Structure of the HIJING/AP/Rcas+ART model.

show the time evolution of the interaction density, scaled to the normal nuclear density $\rho_0 = 0.168$ fm^{-3}, of all baryons in the central cell of a volume $13/\gamma_{cm}$ fm^3 of Au+Au collisions at $\sqrt{s_{NN}} = 19.6$ GeV, averaged over 400 events. Results for the HIJING/AP calculations without (small-dashed lines) and with (solid lines) Regge cascade of initial nucleon interactions are presented. To quantify the impact parameter dependence, we show calculations at fixed impact parameters of 0 and 4 fm. It follows from Fig. 3 that the local baryon and energy densities go down with increasing impact parameter. As one would expect, the influence of Rcas appears in the early stage of the

collision. In the HIJING/AP case, it is seen that a maximum baryon density of about $9\rho_0$ and a maximum energy density of about 4 GeV/fm^3 are reached at about 2 fm/c. Furthermore, maximum baryon and energy densities are reduced to about $8\rho_0$ and 3.5 GeV/fm^3, respectively, when using Rcas. The reduction of the local baryon and energy densities due to Rcas is seen to be large enough to affect the collision dynamics at $t < 10$ fm/c.

Additional information about the importance of Rcas in the high baryon density region can be obtained by calculating the number of particles with local energy densities
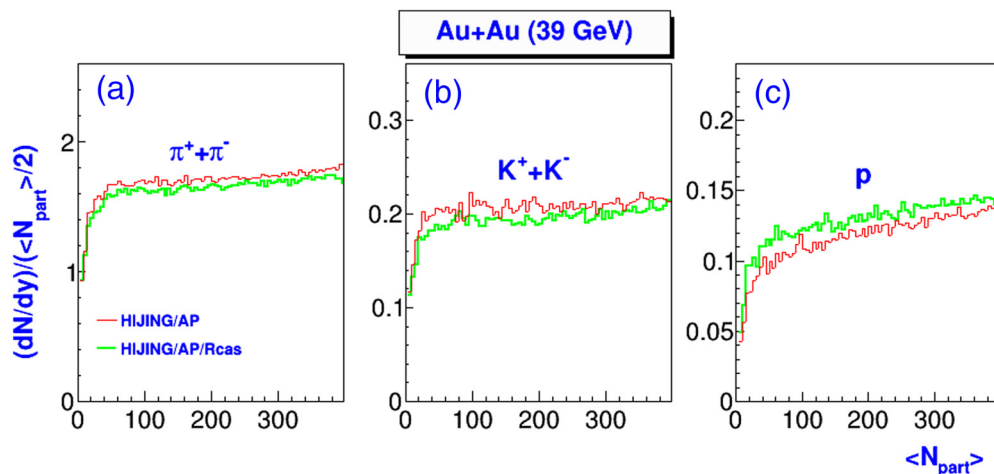

FIG. 2. Multiplicity density dN/dy at mid-rapidity ($|y| < 0.1$) per participant nucleon pair as a function of the average number of participant ($\langle N_{\text{part}} \rangle$) for (a) $\pi^+ + \pi^-$, (b) $K^+ + K^-$, and (c) protons in Au+Au collisions at $\sqrt{s_{NN}} = 39$ GeV. The thick and thin solid lines denote HIJING/AP/Rcas and HIJING/AP calculations, respectively.
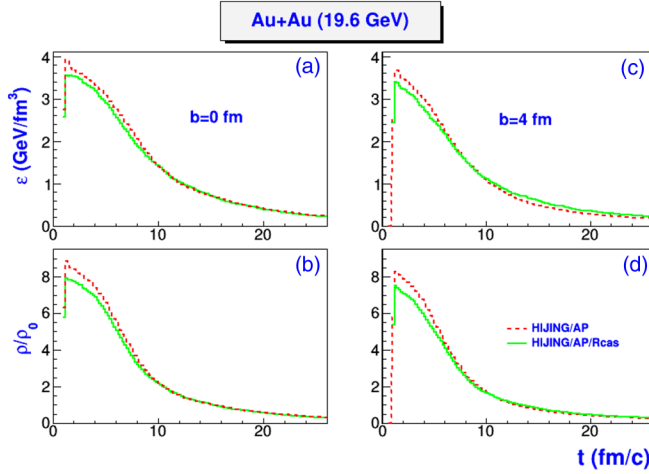
FIG. 3. The evolution of the interaction density and energy densities in a cell of volume $13/\gamma_{cm}$ fm^3 of Au+Au collisions at $\sqrt{s_{NN}} = 19.6$ GeV and impact parameters of 0 and 4 fm. The short-dashed and solid lines denote HIJING/AP and HIJING/AP/Rcas calculations, respectively.

$\varepsilon > 2$ GeV/fm^3. This is shown in Fig. 4. It is seen that the Rcas reduces the number of particles to about 25% at the instant of maximum compression ($\simeq 3$ fm/c), and this reduction persists during the expansion phase, independent of impact parameter. It is also clear that the inclusion of the Rcas mechanism in HIJING/AP calculations reduces the number of particles at both central and semicentral collisions. This is due to the fact that initial cascade is also important in central collision events central collision events [16].

To form a quark-gluon plasma (QGP), it is necessary to achieve an energy density of 1 GeV/fm^3 in the hot fireball produced in high energy nuclear collisions. As shown from Fig. 3, the results obtained from the HIJING/AP(/Rcas) calculations seem to indicate that in central and semicentral Au+Au collisions the conditions for quark-hadron phase transition has indeed been reached at BES energies. However, this also marks the breakdown of the HIJING/AP(/Rcas) model and the need to explicitly include the deconfined quark gluon matter in the model. It was demonstrated in Ref. [26] that the phase structure of strongly interacting matter (QGP) can

TABLE I. Parameter values of HIJING/Rcas.

	C	$\langle p_T^2 \rangle$ (GeV/c)^2	ϵ
Initial-state interactions	0.15	0.5	0.5
Ground state		0.07	0.07

be investigated by a statistical hadronization method. This approach provides a link between data or model calculations of hadron production and the QCD partition functions. This link opens an avenue to shed light on the QCD phase diagram.

In the numerical calculations, the improved HIJING code is run in two modes: standard HIJING 1.383 [7] with the advanced popcorn mechanism of PYTHIA 6.4 [21] (HIJING/AP), and HIJING/AP/Rcas, which incorporates the Regge cascade [16]. In what follows, we denote the improved HIJING calculations with final state interactions as HIJING/AP(/Rcas)+ART. In all calculations, the default HIJING 1.383 [7], PYTHIA 6.4 [21], and ART [5] parameters are selected. We also switch off both parton (jet) shadowing (quenching) and mean field effects. Values of the parameters of different mode choices are listed in Tables I and II. Note that the parameters of HIJING/AP are taken from Ref. [15], which we fit to reproduce the identified hadron rapidity density and transverse mass (m_T) spectra in both peripheral (33%–43%) and central [0%–5(7)%] Pb+Pb collisions at CERN Super Proton Synchrotron (SPS) energies [27–30].

III. RESULTS AND DISCUSSION

In this section we compare three versions of the model in this paper: HIJING/AP, HIJING/AP+ART, and HIJING/AP/Rcas+ART. Detailed descriptions of HIJING, HIJING/AP, and ART models can be found in [5,7,15]. The three versions of the model will be compared with the measured basic bulk observables such as the centrality and energy dependencies of dN/dy, particle ratios, and transverse momentum (p_T) spectra of hadrons—pions, kaons and (anti)protons—at $\sqrt{s_{NN}} = 7.7$, 11.5, 19.6, 27, and 39 GeV, from the STAR BES experiment [1]. The analysis range is
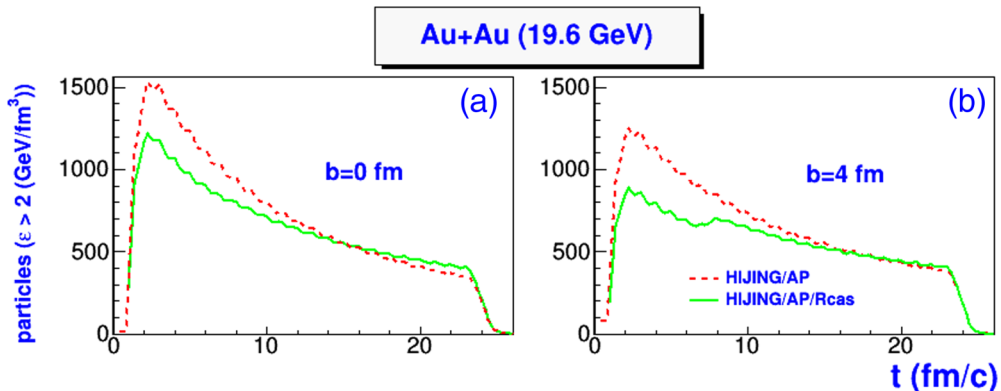

FIG. 4. Same as Fig. 3, but for the particle number.

TABLE II. Parameter values of HIJING/AP

$\gamma_{q'q'}$	γ_s	β_u (GeV^{-1})	$\Delta\beta$ (GeV^{-1})	Δa	ρ (GeV^{-2})	$\sigma'_{q'q'}$ (GeV/c)	α	b (GeV^{-2})
0.2	0.3	1.0	1.2	1.0	0.5	0.648	1.11	0.44

restricted to the measured mid-rapidity range of ($|y| < 0.1$) [1].

The default version of HIJING/AP [15] was constructed to simulate relativistic nucleus-nucleus collisions. Hadronization in the default HIJING/AP is described by the advanced popcorn mechanism [17]. The longitudinal momentum of the hadron is determined by the Lund string fragmentation function [25] with parameters $\alpha = 1.11$ and $b = 0.44$ GeV^{-2}, which work well for both peripheral (33%–43%) and central [0%–5(7)%] Pb+Pb collisions at CERN SPS energies [15]. The production of hadrons is mainly influenced by the diquark p_T kick parameter $\sigma_{q'q'} = 0.36$ GeV/c. In this work, the vertex diquark p_T kick is, however, reduced by $\approx 18\%$ as compared to our previous calculations which underscores the importance of medium effects. Also, a reduction of strangeness suppression factor γ_s by $\approx 23\%$ is found to reproduce the strangeness suppression from the STAR experiment [1].

Before going any further, let us first verify the validity of HIJING/AP, using parameter set of Table II in very peripheral (70%–80%) Au+Au collisions. In this centrality region, HIJING/AP includes no secondary interactions, in either the quark-gluon plasma (QGP) or the hadronic stage. As one can see in Figs. 5 and 6, HIJING/AP (short-dashed lines) is able to reproduce the transverse p_T momentum spectra of the identified hadrons, p, $\pi^\pm$ and $K^\pm$ at various BES energies. It

FIG. 6. Same as Fig. 5, but for (a) π^+, (b) π^-, (c) K^+, and (d) K^-.

was also shown in Fig. 9 of Ref. [15] that HIJING/AP was able to describe the measured rapidity distribution (dN/dy) of $p^\pm$, $\pi^\pm$, and $K^\pm$ in peripheral (30%–40%) Pb+Pb collisions at $\sqrt{s_{NN}} = 17.7$ GeV. This may imply that HIJING/AP provides a unique possibility to explore the initial and final state interaction effects in Au+Au collisions at BES energies, since both effects can be tested while applying the same HIJING/AP code.

Next, in Figs. 7 and 8, we step into central collisions and confront HIJING/AP with the identified hadron spectra at
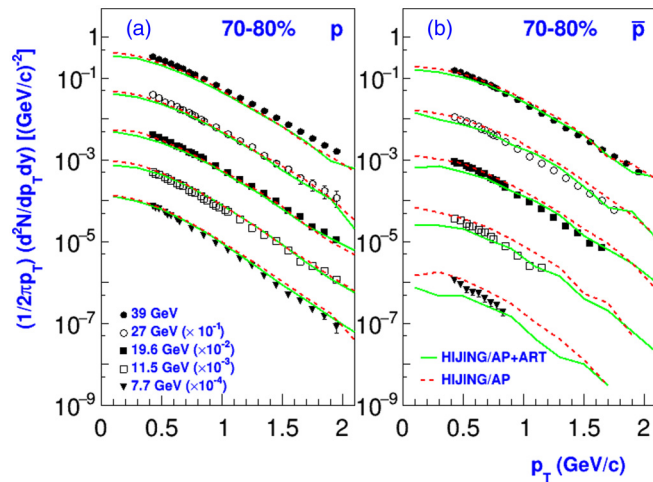

FIG. 5. Mid-rapidity ($|y| < 0.1$) transverse momentum spectra for (a) protons and (b) antiprotons in very peripheral (70%–80%) Au+Au collisions at various BES energies. The sold and short-dashed lines denote HIJING/AP+ART and HIJING/AP calculations, respectively. The closed and open points represent STAR BES data. For illustration purposes, different energies are scaled by different factors.
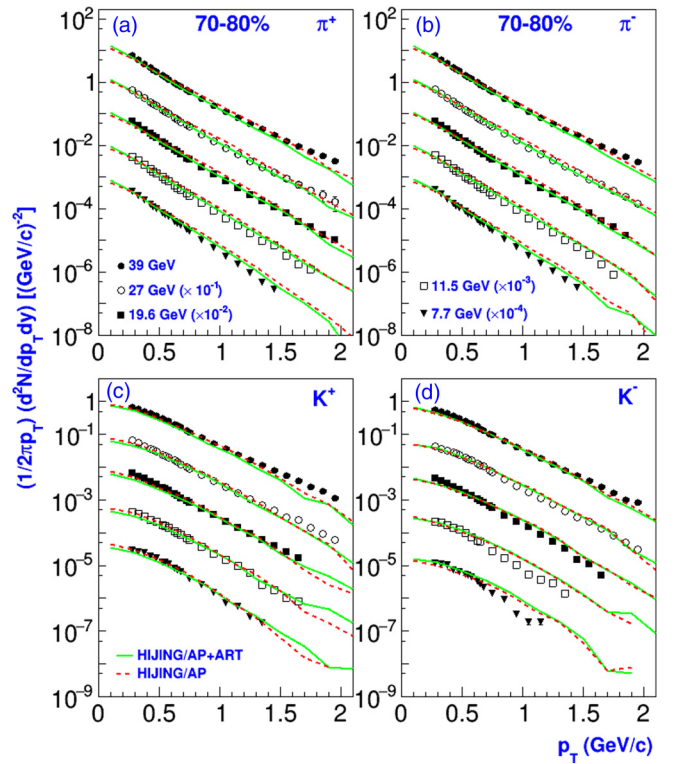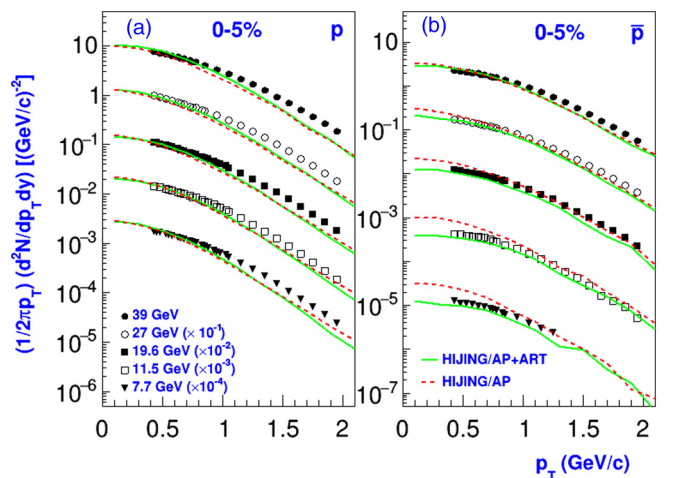

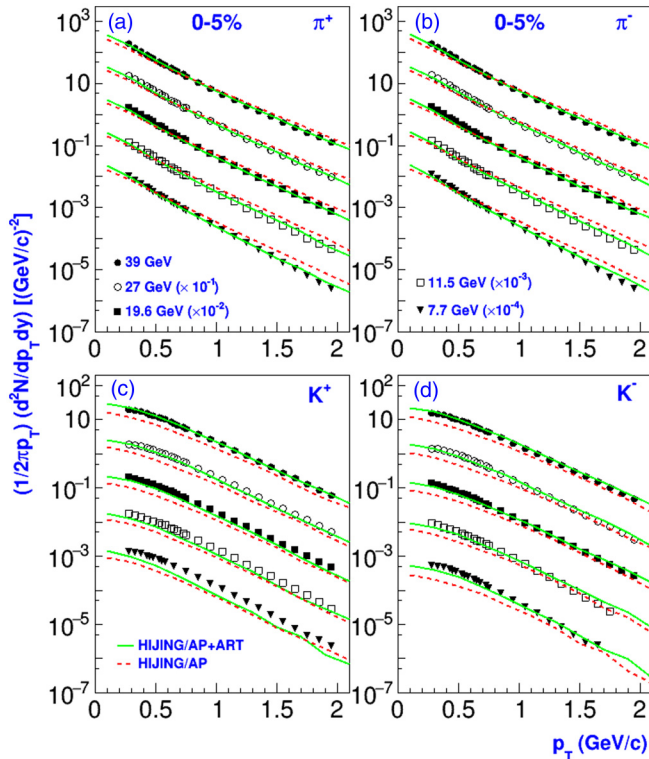FIG. 7. Same as Figs. 5, but for most central (0%–5%) Au+Au collisions.

FIG. 8. Same as Figs. 5, but for (a) π^+, (b) π^-, (c) K^+, and (d) K^- in most central (0%–5%) Au+Au collisions.

various BES energies. We find that HIJING/AP (short-dashed lines) agrees very much with the measured proton spectra, which reflects nuclear stopping, except for a slight overestimation at $p_T > 1$ GeV/c. On the other hand, the HIJING/AP antiproton spectra are consistent with the measured data, especially as the collision energy increases. For the newly produced particles (see Fig. 8) HIJING/AP (short-dashed lines), however, overpredicts the $\pi^\pm$ spectra at large p_T, and lowers the yield of $K^\pm$ at low p_T, especially as the collision energy decreases.

Thus, though HIJING/AP reasonably describes Au+Au stopping at BES energies, it fails to interpret the measured results for the newly produced hadrons. The HIJING/AP+ART and HIJING/AP/Rcas+ART models have been developed to address this failure at STAR BES energies.

The effect of final-state interactions (FSI), realized by HIJING/AP+ART, on the identified hadron spectra, is also investigated in Figs. 5–8 for the two extreme regions of central and very peripheral Au+Au collisions at various BES energies. The solid lines represent the HIJING/AP+ART results. As shown in Figs. 5 and 7 there is little sensitivity to FSI for the proton spectra in central and peripheral Au+Au collisions, as expected. In contrast, HIJING/AP+ART reduces the antiproton yield at low p_T and more closely reproduces the measured spectra, especially in central (0%–5%) collisions over the full p_T range.

For the newly produced particles (see Figs. 6 and 8) the influence of FSI (HIJING/AP+ART) becomes more pro-

nounced in central Au+Au collisions. In particular, FSI decrease the slope of $\pi^\pm$ spectra at large p_T, and increases the $K^\pm$ yield at low p_T, in accordance with the measured data.

Due to the abundant string/minijet production of the beam energy scan (BES) program at the relativistic heavy-ion collider RHIC, mid-rapidity ($|y| < 0.1$) data of identified multiplicity densities (dN/dy) for Au+Au collisions provide a very stringent constrain on medium effects.

In Fig. 9 the measured collision centrality dependence of (dN/dy) of positive (upper panels) and negative (lower panels) particles, normalized by ($\langle N_{\text{part}} \rangle /2$), in Au+Au collisions at $\sqrt{s_{NN}} = 19.6$ and 39 GeV, are compared with the predictions of HIJING/AP (thin lines) and HIJING/AP+ART (thick lines). The data show a continuous increase of the yields of $\pi^\pm$, $K^\pm$, and antiprotons with $\langle N_{\text{part}} \rangle$ and collision energy. However, the proton yields increase with decreasing collision energy. As one can see, HIJING/AP better describes the dependence of (anti)proton and $\pi^\pm$ yields on both $\langle N_{\text{part}} \rangle$ and collision energy. This indicates that the context of fragmentation of strings and minijets in HIJING/AP is enough to explain the increase of charged pions and proton yield with $\langle N_{\text{part}} \rangle$. However, HIJING/AP strongly underestimates the collision centrality dn/dy of strange K^+ and K^- particles at $\langle N_{\text{part}} \gg 200$, which corresponds to 0%–20% centrality.

On the other hand, HIJING/AP+ART (thick lines), with FSI, enhances the production rate of strange particles starting from $\langle N_{\text{part}} \gg 200$, especially as the collision energy increases. However, the HIJING/AP+ART model has developed a broad minimum at $20 < \langle N_{\text{part}} \rangle < 200$ for the (anti)proton yield, indicating that the collisions become quite transparent. This leads to a decrease of the charged pion yield in mid-central ($40 < \langle N_{\text{part}} \rangle < 220$) interactions, especially as the collision energy decreases (see Fig. 9).

In Fig. 10 we study a scenario that would give a larger enhancement of dN/dy of the identified particles. We consider the effect of initial-state interactions as implemented in HIJING/AP/Rcas+ART, and the results are presented in Fig. 10 by thick lines. As one can see, HIJING/AP/Rcas+ART leads to an increase of proton stopping in the mid-central region ($40 < \langle N_{\text{part}} \rangle < 340$), which corresponds to 5%–60% collision centrality, and also provides a better description of dN/dy of charged pions, kaons, and antiprotons. Note that there is no significant difference between HIJING/AP+ART (thin lines) and HIJING/AP/Rcas+ART (thick lines) in peripheral ($N_{\text{part}} < 40$) and central ($N_{\text{part}} > 300$) Au+Au collisions. A similar conclusion is also drawn from the predictions of both models for the p_T spectra of identified particles at the specified centralities (the calculations are not included here).

Figure 10 shows that the inclusion of Rcas in HIJING/AP+ART significantly enhances the production of particles at semicentral collisions. However, it is also demonstrated in Fig. 2 that incorporating Rcas in HIJING/AP is slightly suppressing particle production, when the final hadron rescattering is switched off. It is thus necessary to investigate why Rcas the mechanism brings about two such different scenarios. In Fig. 11 we display the HIJING/AP+ART results with (solid lines) and without (small-dashed lines) Rcas for the evolution of particle number
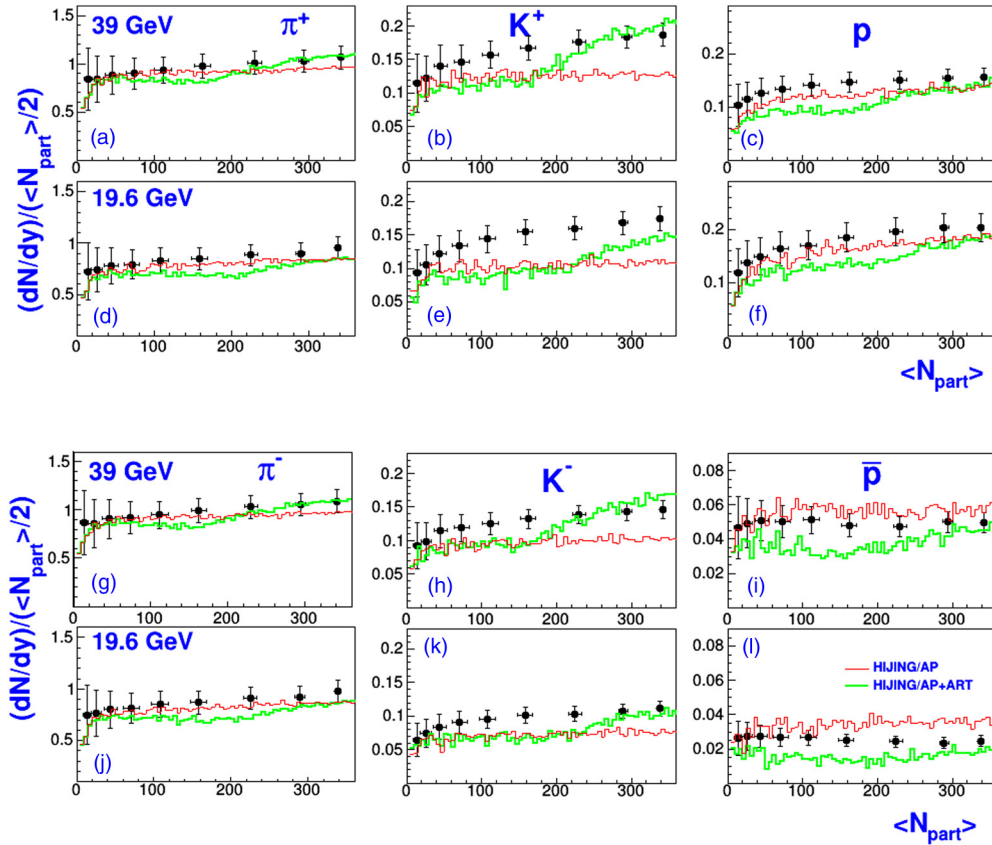
FIG. 9. Centrality dependence of dN/dy per participant pair for charged pions, kaons, and (anti)protons at mid-rapidity ($|y| < 0.1$) in Au+Au collisions at $\sqrt{s_{NN}} = 19.6$ and 39 GeV. The thick and thin solid lines denote HIJING/AP+ART and HIJING/AP calculations, respectively. The solid points with error bars are the STAR BES data. Top panels are for positive particles and lower panels are for antiparticles.

with respect to energy density (ε) at mid-rapidity ($|y| < 0.1$) and fixed impact parameter of $b = 0$, 4, and 7 fm. The left panel of Fig. 11 is for $\varepsilon > 0$ GeV/fm^3 and the right panel is for $\varepsilon > 2$ GeV/fm^3. We shall consider Au+Au collisions at $\sqrt{s_{NN}} = 19.6$ GeV as an example for discussions.

As follows from the left panel of Fig. 11, the particle number with $\varepsilon > 0$ GeV/fm^3 goes down substantially with increasing impact parameter while the duration of the particle number phase is the same. The maximal particle number reached at $t = 16$–24 fm/c is the same in central and semi-central collisions. It is seen that the Rcas leads to a decrease of the particle number for most of the collision times. The importance of Rcas is shown to increase in the region where hadron rescatterings become dominant ($t = 16$–24). This indicates that the dense hadron medium is largely affected by Rcas.

In fact the largest Rcas effects are observed at higher baryon and energy densities of $\rho = 4\rho_0$ and $\varepsilon > 2$ GeV/fm^3, which appears when hadron rescatterings are included. As on can see in the right panel of Fig. 11, there seem to be two distinct regions at about 10 fm/c. In the early stage of the collisions $t < 10$ fm/c, the Rcas significantly reduces the particle number as the impact parameter increases. From Fig. 4, it is clear that this is about the time when most initial nuclear interactions have stopped. In contrast, at $t > 10$ fm/c Rcas generates more particles as more initial nucleon energy

is involved for the final-state hadron productions, especially as the impact parameter increases.

Figure 12 shows the particle ratios model predictions in comparison with data from STAR BES experiment at $\sqrt{s_{NN}} = 39$ GeV. As one can see, HIJING/AP+ART (thin lines), with FSI, underestimates the K^+/π^+ and p/π^+ yields at peripheral and mid-central collisions ($N_{\mathrm{part}} < 240$). In contrast, the clear increase in the K^+/π^+ and p/π^+ ratios, from peripheral to mid-central collisions, is seen to be sensitive to the new physics as implemented in HIJING/AP/Rcas+ART (thick lines). On the other hand, the antiparticle-to-particle ratios show a little sensitivity to the new ingredient implemented in HIJING/AP/Rcas+ART.

The energy dependence of mid-rapidity ($y < |0.1|$) multiplicity density of identified particles and their ratios in central (0%–5%) Au+Au collisions are shown in 13. Solid and short-dashed lines represent the predictions of HIJING/AP/Rcas+ART and HIJING/AP+ART, respectively. As expected, there is little sensitivity to initial-state interactions in central collisions. We can see that HIJING/AP(/Rcas)+ART nicely predicts the increase of the measured yields of charged pions, kaons, and antiprotons with increasing collision energy; see Figs. 13(a), 13(b), and 13(c). Also, the energy dependence trend observed for the proton yield is well described by the model, which reflects the increase in baryon density as the collision energy decreases.
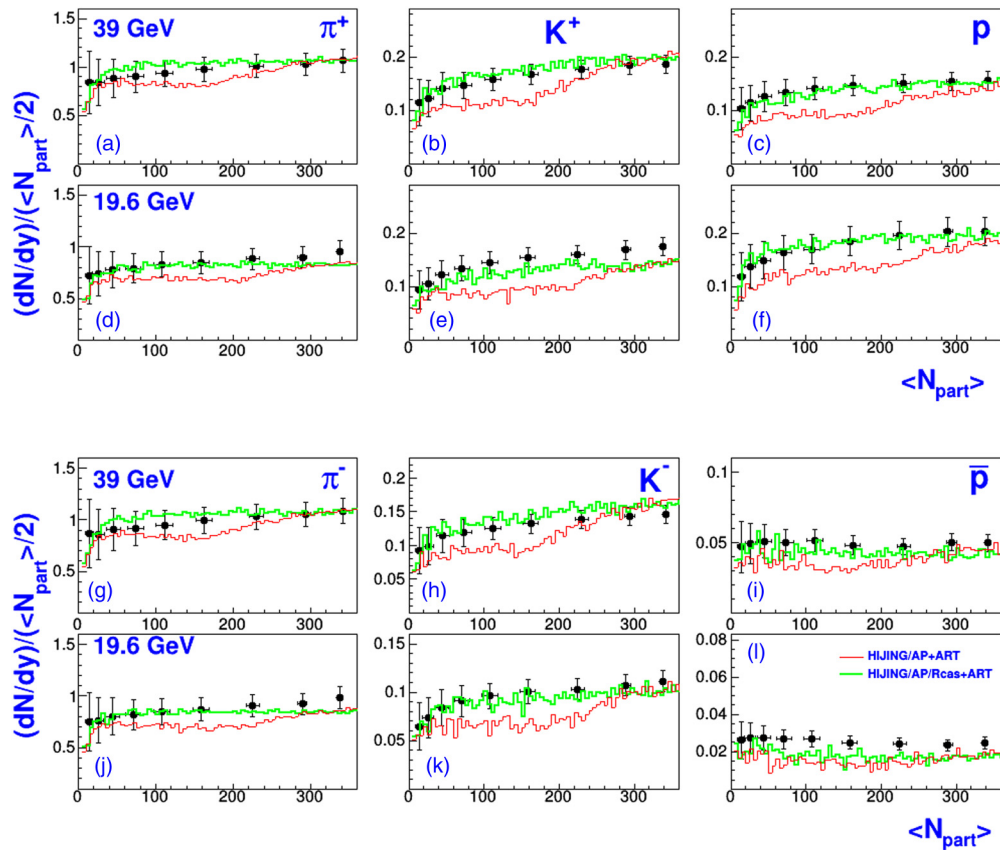
FIG. 10. Same as Fig. 9, but the thin and thick solid lines denote HIJING/AP+ART and HIJING/AP/Rcas+ART, respectively.
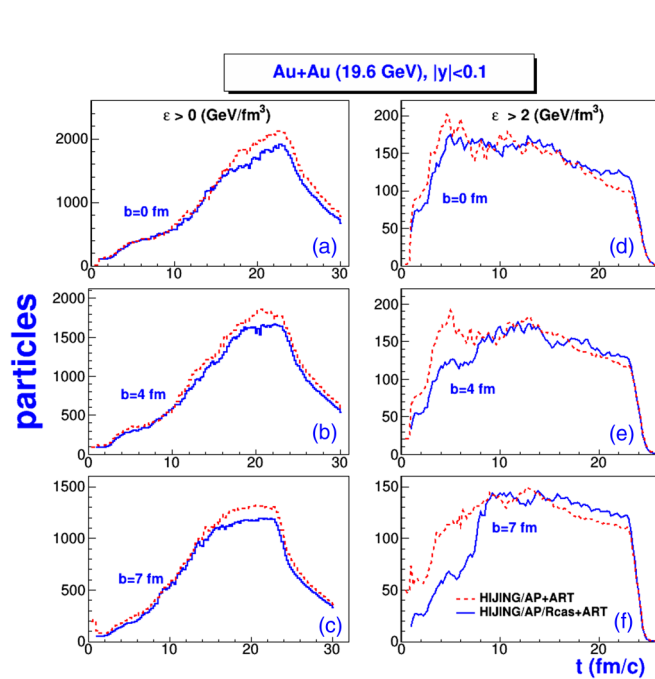

FIG. 11. The evolution of the particle number with respect to energy density (ε) in a cell of volume $13/\gamma_{cm}$ fm^3 of Au+Au collisions at $\sqrt{s_{NN}} = 19.6$ GeV and impact parameters of 0, 4, and 7 fm. The short-dashed and solid lines denote HIJING/AP+ART and HIJING/AP/Rcas+ART calculations, respectively.
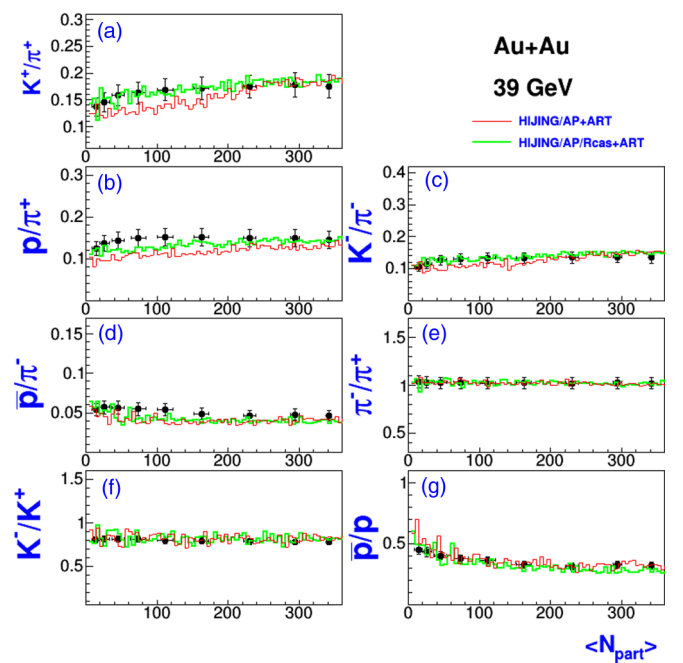

FIG. 12. The centrality dependence of particle ratios in Au+Au collisions at $\sqrt{s_{NN}} = 39$ GeV. The thick and thin solid lines denote HIJING/AP/Rcas+ART and HIJING/AP+ART calculations, respectively. The solid points with error bars are the data from the STAR BES experiment.
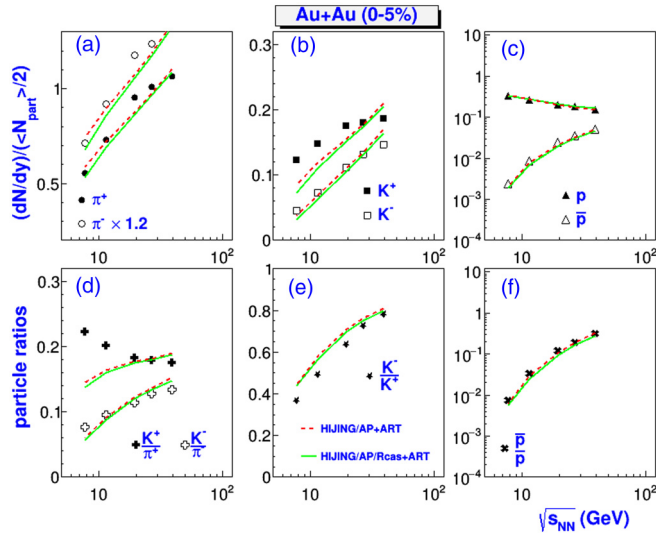
FIG. 13. The energy dependence of multiplicity density dN/dy per participant pair (upper panel) and particle ratios (lower panel) in most central (0%–5%) Au+Au collisions. The thick and thin solid lines denote HIJING/AP/Rcas+ART and HIJING/AP+ART calculations, respectively. The points with error bars are the data from the STAR BES experiment.

It should be pointed out that AMPT code [14] also uses an intermediate step, between HIJING [7] and ART [5] codes, to model the sharp increase of partonic energy density during the first few fm/c of the collision. It is assumed that strings (minijet partons) can lose energy by scattering of quarks/antiquarks (minijet gluons) of all flavors, using Zhang's parton cascade [8] model. After parton stop interacting, hadronization of these strings are described by Lund string fragmentation or a simple quark coalescence models [6,14]. It was shown in Ref. [13] that the AMPT model with default and string melting versions (that include quark/gluon scatterings) could not consistently describe the centrality dependence of multiplicity density dN/dy, particle ratios of Au+Au collisions at $\sqrt{s_{NN}} = 7.7$, 27, and 200 GeV.

IV. SUMMARY AND CONCLUSIONS

We studied, in the framework of the HIJING/AP model, the influence of initial- and final-state interactions on new experimental observables measured by STAR Collaboration, especially for the identified particles $\pi^{\pm}$, $K^{\pm}$, and (anti)protons in Au+Au collisions at $\sqrt{s_{NN}} = 7.7$, 11.5, 19.6, 27, and 39 GeV. The Regge cascade (Rcas) recipe initiate interactions among the primary and noninteracting nucleons of the projectile/target. The energy loss of excited strings and minijets is implicitly taken into account through an effective transfer of momentum/energy of the primary interacting nucleons to the surrounding ones. The final-state interactions are treated via a relativistic transport (ART) model of hadronic scatterings. From the model calculations we can draw the following conclusions:

(i) For the transverse (p_T) momentum of protons, charged pions, and kaons in very peripheral (70%–80%) Au+Au collisions, HIJING/AP results with and without final-state interactions are close together and can describe the corresponding experimental data for all the p_T range at various BES energies. This implies that the bulk dynamics within HIJING/AP approach are verified, and the model provides a unique possibility to explore medium effects in Au+Au collisions at BES energies.

(ii) HIJING/AP with final-state interactions lowers the yield of antiprotons at low p_T in central (0%–5%) Au+Au collisions, which is favored by experimental data at low BES energies.

(iii) For the newly produced charged pions and kaons in central collisions at various BES energies, the sensitivity to the final-state interactions is visible at both low and large p_T values, and more closely reproduces the experimental data.

(iv) The centrality dependence of dN/dy of $\pi^{\pm}$, $K^{\pm}$, p, and $\bar{p}$ at $\sqrt{s_{NN}} > 11.5$ is found to be quite sensitive to the details of initial- and final-state interaction effects: the inclusion of initial-state interactions considerably improves the description of data to large extent.

(v) The introduction of initial-state interactions improves the yield of mixed ratios ($K^{\pm}/\pi^{\pm}$ and $p^{\pm}/\pi^{\pm}$)

From Fig. 13(b) one can also see that the model reproduces rather well the energy dependence of K^- yield, but the results strongly underestimate the K^+ yield as the collision energy decreases. It should be noted that, there is a significant difference between K^+ and K^- production mechanisms in the HIJING/AP(/Rcas)+ART model. At the studied BES energies, K^+ production is a result of an interplay between resonance production and color string fragmentation, while K^- production is dominated by string fragmentation. The resonance production dominates at $\sqrt{s_{NN}} \leqslant 11.5$ GeV, and treated by the ART model [5], as a result of the reactions $NN \rightarrow KYN$, $\pi N \rightarrow KY$, where Y is a hyperon. While at higher energies ($\sqrt{s} = 5$ GeV for baryon-baryon and 3 GeV for meson-baryon and meson-meson interactions) excited strings are formed and they decay into hadrons according to the advanced popcorn [17] of the Lund string fragmentation model [25].

Figures 13(d), 13(e), and 13(f) show the collision energy dependence of the particle ratios $K^{\pm}/\pi^{\pm}$, K^-/K^+, and $\bar{p}/p$ in central collisions. As one can see, the HIJING/AP(/Rcas)+ART results follow the same trend as the measured ratios K^-/π^-, K^-/K^+, and $\bar{p}/p$. However, the model gives a partial agreement of K^-/K^+ ratios at low BES energies, in the region where a significant contribution of K^+ production from resonance particles is expected. On the other hand, the model can describe the low $\bar{p}/p$ ratios at low BES energies, i.e., the large stopping at these energies, but fails to describe the energy dependence of K^+/π^+ at $\sqrt{s_{NN}} \leqslant 11.5$ GeV. An enhancement of K^+/π^+ ratios at low BES energies reflects the strangeness content relative to entropy in Au+Au collisions, which may be taken as a signature of QGP formation.

especially in peripheral and mid-central collisions ($N_{part} < 250$).

(vi) The observed trend of the energy dependence of particle yields ($\pi^{\pm}$, $K^{\pm}$, $p^{\pm}$) and particle ratios (K^+/π^+, K^-/K^+, and $\bar{p}/p$) in central (0%–5%) Au+Au collisions, is well described by the HIJING/AP(/Rcas)+ART model that incorporate both initial- and final-state interactions.

Therefore, HIJING/AP model is extended to include the Regge cascade recipe for the initial-state interactions as well as adding ART for hadronic rescattering. These modifications make improvements in the full event Monte Carlo description of Au+Au collisions at BES energies. The new version can account for many features of multiplicity density dN/dy and particle ratios in peripheral and mid-central Au+Au colli-sions. A simultaneous reproduction of bulk properties such as dN/dy, particle ratios, and transverse momentum of charged pions, kaons, and (anti)protons in Au+Au collisions at BES energies, which is a challenge of HIJING type like models, is well described within HIJING/AP/Rcas+ART. One of the remaining discrepancies is the enhancement of K^+/π^+ at low BES energies, which will require further investigation.

[1] L. Adamczyk *et al.* (STAR Collaboration), Phys. Rev. C **96**, 044904 (2017).

[2] H. Sorge, Phys. Rev. C **52**, 3291 (1995).

[3] S. Bass *et al.*, Prog. Part. Nucl. Phys. **41**, 255 (1998).

[4] S. H. Kahana, D. E. Kahana, Y. Pang, and T. J. Schlagel, Annu. Rev. Nucl. Part. Sci. **46**, 31 (1996).

[5] B. A. Li and C. M. Ko, Nucl. Phys. A **630**, 556 (1998).

[6] Z. W. Lin and C. M. Ko, Phys. Rev. C **65**, 034904 (2002).

[7] X. N. Wang and M. Gyulassy, Phys. Rev. D **44**, 3501 (1991).

[8] B. Zhang, Comput. Phys. Commun. **109**, 193 (1998).

[9] B. Andersson, G. Gustafson, and B. Nilsson-Almqvist, Nucl. Phys. B **281**, 289 (1987).

[10] B. Nilsson-Almqvist and E. Stenlund, Comput. Phys. Commun. **43**, 387 (1987).

[11] T. Sjostrand, Comput. Phys. Commun. **82**, 74 (1994).

[12] H.-U. Bengtsson and T. Sjostrand, Comput. Phys. Commun. **46**, 43 (1987).

[13] A. Nandi, L. Kumar, and N. Sharma, Phys. Rev. C **102**, 024902 (2020).

[14] Z. W. Lin, C. M. Ko, B. A. Li, B. Zhang, and S. Pal, Phys. Rev. C **72**, 064901 (2005).

[15] K. Abdel-Waged and N. Felemban, J. Phys. G: Nucl. Part. Phys. **47**, 065104 (2020).

[16] K. Abdel-Waged and N. Felemban, J. Phys. G: Nucl. Part. Phys. **45**, 025104 (2018).

[17] P. Edén and G. Gustafson, Z. Phys. C **75**, 41 (1997).

[18] K. Abdel-Waged and V. V. Uzhinskii, Yad. Fiz. **60**, 925 (1997) [Phys. Atom. Nucl. **60**, 828 (1997)].

[19] K. Abdel-Waged and V. V. Uzhinskii, J. Phys. G: Nucl. Part. Phys. **24**, 1723 (1998).

[20] K. Abdel-Waged and N. Felemban, Phys. Rev. C **91**, 034908 (2015).

[21] T. Sjostrand, S. Mrenna, and P. Skands, J. High Energy Phys. 05 (2006) 026.

[22] B. Andersson, G. Gustafson, and T. Sjostrand, Nucl. Phys. B **197**, 45 (1982).

[23] B. Andersson, G. Gustafson, and T. Sjostrand, Phys. Scr. **32**, 574 (1985).

[24] J. S. Schwinger, Phys. Rev. **82**, 664 (1951).

[25] B. Andersson, G. Gustafson, and B. Soderberg, Z. Phys. C **20**, 317 (1983).

[26] A. Andronic, P. Braun-Munzinger, K. Redlich, and J. Stachel, Nature (London) **561**, 321 (2018).

[27] T. Anticic *et al.* (NA49 Collaboration), Phys. Rev. C **83**, 014901 (2011).

[28] T. Anticic *et al.* (NA49 Collaboration), Phys. Rev. C **86**, 054903 (2012).

[29] S. V. Afanasiev *et al.* (NA49 Collaboration), Phys. Rev. C **66**, 054902 (2002).

[30] C. Alt *et al.* (NA49 Collaboration), Phys. Rev. C **73**, 044910 (2006).